ELSEVIER

Colloids and Surfaces A: Physicochem. Eng. Aspects 256 (2005) 91–103

COLLOIDS AND SURFACES A

www.elsevier.com/locate/colsurfa

Finite element estimation of electrostatic double layer interaction between colloidal particles inside a rough cylindrical capillary: effect of charging behavior

Prodip K. Das, Subir Bhattacharjee*

Department of Mechanical Engineering, 4-9 Mechanical Engineering Building, University of Alberta, Edmonton, AB, Canada T6G 2G8

Received 12 August 2004; accepted 29 December 2004

Abstract

In this paper, we present the electrostatic double layer (EDL) interactions between colloidal particles trapped inside a rough cylindrical capillary based on finite element analysis of the governing Poisson–Boltzmann equation. The effective EDL force between the particles is evaluated for different combinations of charging behavior (constant potential and constant surface charge density) of the particles and the capillary wall. Effect of capillary wall roughness is estimated using a simple model of a rough surface, which assumes the capillary wall to be a periodic function of axial position. The interaction force experienced by the particles was affected significantly by the proximity of the rough capillary wall, the charging behavior of the particles and the capillary wall, as well as the amplitude and frequency of the wall roughness.

Keywords: Colloidal particle; Capillary; Electrostatic double layer interactions; Finite element analysis; Poisson–Boltzmann; Surface roughness

1. Introduction

The Derjaguin–Landau–Verwey–Overbeek (DLVO) interaction between colloidal particles is of paramount importance for understanding many natural and industrial processes involving colloidal dispersions, such as flow through porous media, deposition of particles, capillary electrophoresis, chromatographic separations, micro-fluidic actuation, and membrane separations [1–4]. In the DLVO theory, it is assumed that the interacting bodies are in an infinite medium. However, in real systems, most colloidal interactions occur in confined domains, like porous media or microscopic channels, where particles simultaneously interact with other particles and the wall of the confining geometry. In addition to confinement, all surfaces are inherently rough at small length scales, which can significantly modify the nature of the interactions. For instance, surface roughness is typically considered as a possible cause for the large discrepancies observed between the theoretical predictions and experimental observations in particle deposition, hetero-coagulation, colloidal fouling of surfaces, and various others engineered and natural processes [5–12].

During the past several decades, considerable attention has been devoted toward accurate prediction of colloidal interactions for various geometries, for instance, particle–particle interaction in infinite domains, particle–plate interaction, and interaction between a particle with cylindrical capillary [13–22]. However, particle–particle interactions in confined domains have not been studied as rigorously. Calculations of the net electrostatic double layer (EDL) interaction in such confined geometries is a non-trivial problem that requires addressing the electrostatic interactions in a “three-body” system comprised of the two particles and the wall of the confining domain. In a confined system, the presence of charge on the confining walls alters the electrolyte

* Corresponding author. Tel.: +1 780 492 6712; fax: +1 780 492 2200.
E-mail address: subir.b@ualberta.ca (S. Bhattacharjee).

0927-7757/$ – see front matter © 2005 Elsevier B.V. All rights reserved.
doi:10.1016/j.colsurfa.2004.12.059

Nomenclature

a	radius of the particle
A	size ratio (= b/a)
b	mean radius of the rough capillary
e	electronic charge (1.6×10^{-19} C)
$\mathbf{E}$	electrostatic field vector
E_r, E_z	components of the electric field vector along the r- and z-directions, respectively
F	force
f_z	scaled force acting along the z-direction
F_z	component of force acting along the z-direction
h	surface-to-surface separation distance between particles
i	index number (0 to n)
$\mathbf{I}$	identity tensor
k	Boltzmann constant (1.38×10^{-23} J K^{-1})
$\mathbf{k}$	unit vector in the positive z-direction
$\mathbf{n}$	unit surface normal vector
n_∞	ionic number concentration in the bulk solution (m^{-3})
n_r, n_z	components of the unit surface normal along the r- and z-directions, respectively
q_p	surface charge density (C m^{-2})
r	radial coordinate in the cylindrical coordinate system
S	semicircular boundary of the spherical particle
T	temperature (K)
$\mathbf{T}_{ij}$	component of stress tensor
z	axial coordinate in the cylindrical coordinate system

Greek symbols

α	amplitude of the rough capillary
$\partial\Omega$	boundary of the computational domain
ε_0	dielectric permittivity of vacuum (8.8542×10^{-12} C^2 N^{-1} m^{-2})
ε	dielectric constant of the suspending fluid
κ	inverse of Debye screening length, Eq. (3)
λ	wavelength of the rough capillary
η	scaled amplitude
ν	absolute value of the valency for a symmetric (ν·ν) electrolyte solution
Π	osmotic pressure
σ_c	scaled surface charge density of capillary wall
σ_p	scaled surface charge density of particle
ψ	electric potential (V)
Ψ	scaled potential (=$\nu e\psi/kT$)
Ψ_p,Ψ_c	scaled surface potentials of particle and capillary, respectively
$\Psi_{p,\infty}$	scaled surface potential of an isolated spherical particle
ξ	scaled wavelength

Abbreviations

CC	constant charge
CP	constant potential
DLVO	Derjaguin–Landau–Verwey–Overbeek
EDL	electrostatic double layer
PB	Poisson–Boltzmann

distribution inside the domain, which in turn influences the net electrostatic interaction between two colloidal particles in the confinement [23]. Furthermore, if the walls of the confinement are rough, the electrolyte distribution is perturbed locally, which can cause further complications. The overall consequence is that the EDL interactions between colloidal particles in complex confined geometries cannot be determined by commonly used pairwise summation of the particle–particle and particle–wall interactions.

In this article, we use a previously developed model problem of two spherical colloidal particles inside a cylindrical micro-capillary of comparable dimensions, with a periodic undulation present on the capillary wall [24]. This problem is a simple mathematical construct to assess the coupled influence of the charged capillary wall, as well as surface roughness of the wall, on the electrostatic interaction between the colloidal particles. Available techniques to calculate the interactions between rough surfaces are mainly limited to the pair interaction between two particles or particle-plate interaction in an infinite medium [12,25–29]. Roughness of the confining domain, and its influence on the EDL interaction between the confined particles has only been studied recently, and that too, for constant potential particles [24]. The importance of considering roughness on confining walls of a capillary stems from our attempts to analyze the flow of particles inside microscopic micro-fluidic channels. Typical micro-fabrication practices, which involve etching the channels on a suitable substrate, rarely yield smooth walls [24]. In many cases, the roughness of the walls is substantial, and adversely influences the manipulation of the particles by altering the electrical field distributions in the channel.

Here, we present finite element simulation results depicting how presence of roughness on the confining walls can influence the electrostatic forces between two confined particles for different combinations of charging behavior (constant potential and constant surface charge density) on the surfaces involved. The roughness is modeled as a periodic oscillation in the capillary wall radius with various amplitude and pitch, thus emulating a wide variety of roughness features. These simulation results indicate the profound influence of the wall roughness on the particle-particle interaction force, and how such roughness features coupled with different charging behaviors of the surfaces can engender significant alterations in the electrostatic forces experienced by the particles.

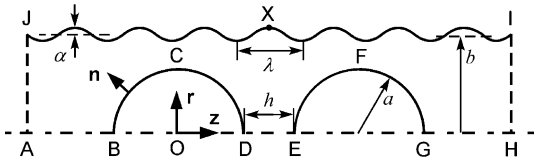

Fig. 1. Schematic representation of computational domain for simulating the interaction between two spherical particles of radius a inside a rough cylindrical capillary of mean radius b, amplitude α and wavelength λ. The arcs BCD and EFG represent the particle surfaces; IJ represents the undulation of the capillary, and AH is the axis of symmetry. Point X is located at the middle of the channel aligned with a crest of the undulation. The particles are moved equal distances from this reference point to attain different values of κh.

2. Problem description and governing equations

2.1. Model geometry and Poisson–Boltzmann equation

In this section, we present a brief description of the mathematical formulation, and some key steps used in the numerical solution technique. A detailed description of the numerical procedures is available elsewhere [23,24]. Fig. 1 shows the cylindrical geometry under consideration in the present investigation along with the coordinate framework. Here, two charged spherical colloidal particles of radius a are separated by a distance h (distance of closest approach) in an infinitely long wavy capillary of mean radius b and amplitude α. The wavy pattern on the capillary wall is represented using Bézier curves. The procedure of generating such features is described in our previous work [24].

The electric double layer formed around the particles due to the interaction of the ionized solution with the charged particles in a dielectric medium is governed by the Poisson–Boltzmann (PB) equation:

$$\varepsilon\varepsilon_0\nabla^2\psi = -\sum_{i=1}^{n} n_{i\infty}\nu_i e \exp\left(-\frac{\nu_i e\psi}{kT}\right) \tag{1}$$

Here ε is the dielectric constant of the suspending fluid, ε_0 is the dielectric permittivity of vacuum, ψ is the electric potential expressed in Volts. The right hand side of Eq. (1) represents the volumetric charge density in the domain, which is given by Boltzmann distribution of the ions in the diffuse double layer. The bulk solution ionic number concentration is $n_{i\infty}$, ν_i is the charge number of the ith ionic species, e is the magnitude of the electronic charge, k is the Boltzmann constant, and T is the absolute temperature. Assuming a symmetric electrolyte ($\nu_+ = -\nu_- = \nu_i = \nu$; $n_{i\infty} = n_\infty$), Eq. (1) is further simplified as [30]

$$\nabla^2\Psi = \kappa^2 \sinh(\Psi) \tag{2}$$

where Ψ ($=\nu e\psi/kT$) is the scaled potential and the parameter κ is the inverse Debye screening length, defined as

$$\kappa = \left(\frac{2n_\infty e^2\nu^2}{\varepsilon\varepsilon_0 kT}\right)^{1/2} \tag{3}$$

Eq. (2) is valid within the electrolyte medium, i.e., outside the charged bodies. The particles and the capillary are assumed to be perfect dielectrics, and hence, we only solve the PB equation in the symmetric electrolyte medium. Here, we considered three different combinations of charged bodies, namely: (i) two constant charge (CC) particles inside a constant potential (CP) rough capillary; (ii) a CC and a CP particle inside a CP rough capillary; and (iii) two constant charge (CC) particles inside a constant charge (CC) rough capillary.

2.2. Boundary conditions

Depending on the charging behavior of the surfaces immersed in the dielectric, the electrostatic boundary conditions at the solid liquid interfaces can be treated as constant surface potential, constant surface charge, or surface charge regulation conditions [13,16,31]. Usually, most charged interfaces in aqueous electrolyte media tend to obey some form of a charge regulatory behavior. However, it is known that constant potential (CP) and constant charge (CC) conditions represent the limiting charging behaviors of the interfaces, and provide a lower and an upper bound of the interaction, respectively [16]. Accordingly, we only explore the cases of CP and CC boundary conditions, expecting that these results will reflect the liming behavior of the electrostatic double layer interactions. In our earlier study [24], we presented the interaction forces between two CP particles inside a CP capillary. In the present investigation, we consider different combinations of CP and CC conditions at the solid liquid interfaces. We also consider the interactions when all the surfaces have CC conditions.

For the case of CC particles and CP capillary, the boundary condition on the particle surfaces is defined as

$$-\mathbf{n}\cdot\nabla\Psi = \sigma_\mathrm{p} \text{ for } \partial\Omega \in \text{BCD and EFG} \tag{4}$$

where $\mathbf{n}$ is the unit normal to the particle–electrolyte interface pointing to the electrolyte, and σ_p is the scaled surface charge density, related to the interfacial charge density q_p (C m^{-2}) as

$$\sigma_\mathrm{p} = \frac{\nu e q_\mathrm{p}}{\kappa\varepsilon\varepsilon_0 kT} \tag{5}$$

Here, the interfacial surface charge density of the particles is related to the surface potential on the spherical particles in isolation through [32]

$$\begin{aligned} q_\mathrm{p} &= \frac{Q_\mathrm{p}}{4\pi a^2} \\ &= \frac{\kappa\varepsilon\varepsilon_0 kT}{\nu e}\left[2\sinh\left(\frac{1}{2}\Psi_{\mathrm{p},\infty}\right) + \frac{4}{\kappa a}\tanh\left(\frac{1}{4}\Psi_{\mathrm{p},\infty}\right)\right] \end{aligned} \tag{6}$$

where Q_p is the total surface charge, and $\Psi_{\mathrm{p},\infty}$ is the surface potential of an isolated spherical particle. This semi-empirical relationship gives the charge density to within 5%

of the exact charge density on an isolated sphere for $\kappa a > 0.5$ for any surface potential. Thus, known values of the surface potential on a particle in isolation will provide the necessary constant charge boundary conditions at the particle surfaces.

The boundary condition on the constant potential capillary wall surface is

$$\Psi = \Psi_c \text{ for } \partial\Omega \in \text{IJ} \tag{7}$$

while the remaining parts of the geometry (Fig. 1) are subjected to symmetry boundary conditions

$$\mathbf{n} \cdot \nabla\Psi = 0 \text{ for } \partial\Omega \in \text{all other segments} \tag{8}$$

This statement implies that the potential gradients normal to these line segments are zero, where **n** represents the unit normal to the surface. Clearly, this is an artificial boundary condition on the segments JA and HI, and appropriate measures must be taken in the numerical solution to ensure that this artificial boundary condition does not influence the accuracy of the solution. The above construction provides the generalized formulation of the electrostatic problem. Solution of the PB equation in a given geometrical framework requires recasting Eq. (2) in the proper coordinate system representing the geometry. Detailed formulations and necessary normalizations are described elsewhere [23].

When one or both of the particle surfaces have constant surface potential, we replace the boundary condition, Eq. (4), by a CP condition, given by

$$\Psi = \Psi_p \text{ for } \partial\Omega \in \text{BCD and/or EFG} \tag{9}$$

where Ψ_p is the potential on the particle surface.

2.3. Force calculation

From the potential distribution obtained by solving the Poisson–Boltzmann equation with appropriate boundary conditions, the electrostatic force on the spherical particles is calculated by integrating the total stress tensor, defined as

$$\mathbf{T}_{ij} = \left(\Pi - \frac{1}{2}\varepsilon\varepsilon_0\mathbf{E}\cdot\mathbf{E}\right)\mathbf{I} + \varepsilon\varepsilon_0\mathbf{E}\mathbf{E} \tag{10}$$

over the surface of a particle, yielding

$$\mathbf{F} = \iint_S \mathbf{T}_{ij}\cdot\mathbf{n}\,\mathrm{d}S = \iint_S \left[\left(\Pi - \frac{1}{2}\varepsilon\varepsilon_0\mathbf{E}\cdot\mathbf{E}\right)\mathbf{I} + \varepsilon\varepsilon_0\mathbf{E}\mathbf{E}\right]\cdot\mathbf{n}\,\mathrm{d}S \tag{11}$$

Here **F** is the force acting on the spherical particle, $\mathbf{T}_{ij}$ is the stress tensor, **E** ($=-\nabla\psi$) is the electrostatic field vector, Π is the osmotic pressure difference between the electrolyte at the particle surface and the bulk solution, **n** is the unit outward surface normal, and **I** represents the identity tensor.

The net force acting on a sphere along the axial (z) direction is determined from the component of Eq. (11) acting along the z-direction and can be written explicitly as

$$F_z = \mathbf{F}\cdot\mathbf{k} = 2\pi\kappa^2\varepsilon\varepsilon_0\left(\frac{kT}{ve}\right)^2\int_s\left[n_z\left\{(\cosh\Psi - 1) + \frac{1}{2}(E_z^2 - E_r^2)\right\} + n_r E_r E_z\right] r\,\mathrm{d}r \tag{12}$$

where the subscript S represents integration over the closed surface of the particle. This integration can be performed on either of the two particles. In the above expression, F_z is the force acting along the z-direction, **k** is a unit vector in the positive z-direction, n_r and n_z are the components of the unit surface normal vector **n** along the r- and z- directions, respectively. E_r and E_z are the components of the electric field vector **E** along the r- and z- directions, respectively. The term $(\cosh\Psi - 1)$ in Eq. (12) represents the osmotic pressure contribution to the net EDL force, while the two remaining terms in the square brackets represent the electrostatic (Maxwell) stress. Finally, the axial force is represented in its non-dimensional form, given by

$$f_z = \frac{F_z}{\varepsilon\varepsilon_0}\left(\frac{ve}{kT}\right)^2 \tag{13}$$

We note here that the force is calculated on the sphere BCD with its center at the origin. Therefore, a repulsive force will be directed toward the negative z-direction, while an attractive force will act along the positive z-direction. In some instances, the force is also calculated on the sphere EFG, where repulsive force will be directed toward the positive z-direction. In the results presented, a negative value of the force implies

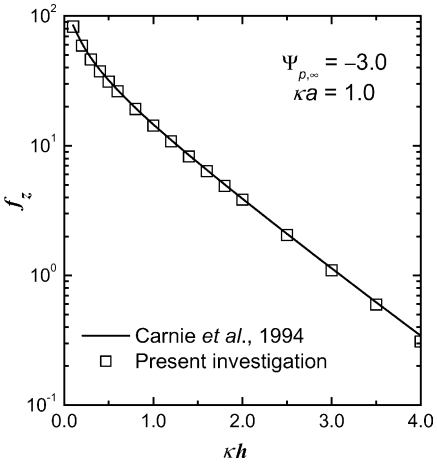

Fig. 2. Comparison between finite element results obtained in this study with the finite difference results based on a Hermite collocation technique in a bispherical coordinate system. Symbols represent the finite element results of the electrostatic interaction force between two constant charge (CC) particles in an unbounded electrolyte with scaled separation distance (κh). The line represents the finite difference collocation results. In the finite element solutions, the charge density on the particles was evaluated employing Eq. (6) using a surface potential $\Psi_{p,\infty} = -3.0$, while in the finite difference collocation method it was obtained by numerically solving the PB equation around an isolated particle. The parameter κa is 1.0 in this and all subsequent figures.

Table 1
Steps of the finite element adaptive mesh refinement scheme showing the convergence of the scaled EDL force (f_z) between two constant charge spherical particles with mesh refinements

Smooth capillary ($\eta = 0.0$)			Rough capillary ($\xi = 1.0$, $\eta = 0.1$)		
No. of elements	Global error	EDL force (f_z)	No. of elements	Global error	EDL force (f_z)
1635	0.048077	15.416	1530	0.208299	19.005
3862	0.015875	15.528	3772	0.026864	19.276
8248	0.004868	15.494	8766	0.006949	19.220
18397	0.001545	15.491	20267	0.002344	19.275
37865	0.000520	15.489	45119	0.000713	19.251

$\Psi_{p,\infty} = -3.0$, $\Psi_c = -3.0$, $\kappa h = 0.4$.

attraction, while positive value represents repulsion for all cases.

2.4. Numerical solution

The numerical solution of the governing equations was performed using a finite element software (FEMLAB®, Comsol Inc.). Details of the numerical computation are given in [23]. Briefly, the non-dimensionalized PB equation was written in an axisymmetric cylindrical coordinate system, with all the lengths scaled with respect to the screening length of the EDL interactions. In the scaled problem, the particle radius was always fixed as $\kappa a = 1$ and the capillary radius was set to $\kappa b = 1.2$. The roughness parameters α and λ were scaled with respect to the particle radius a. In the parametric studies, the scaled wavelength of the roughness, $\xi = \lambda/a$, was varied between 0.4 and 4. The scaled amplitude, $\eta = \alpha/a$, was varied from 0 (smooth capillary wall) to 0.15. For all simulations, the boundaries AJ and HI were placed at least two particle radii away from the outer edges of the particles to ensure that their presence does not influence the interaction force calculations. The forces were calculated for different separations between the two particles. In these calculations, it was ensured that the contact between the two particles ($\kappa h = 0$) always occurs

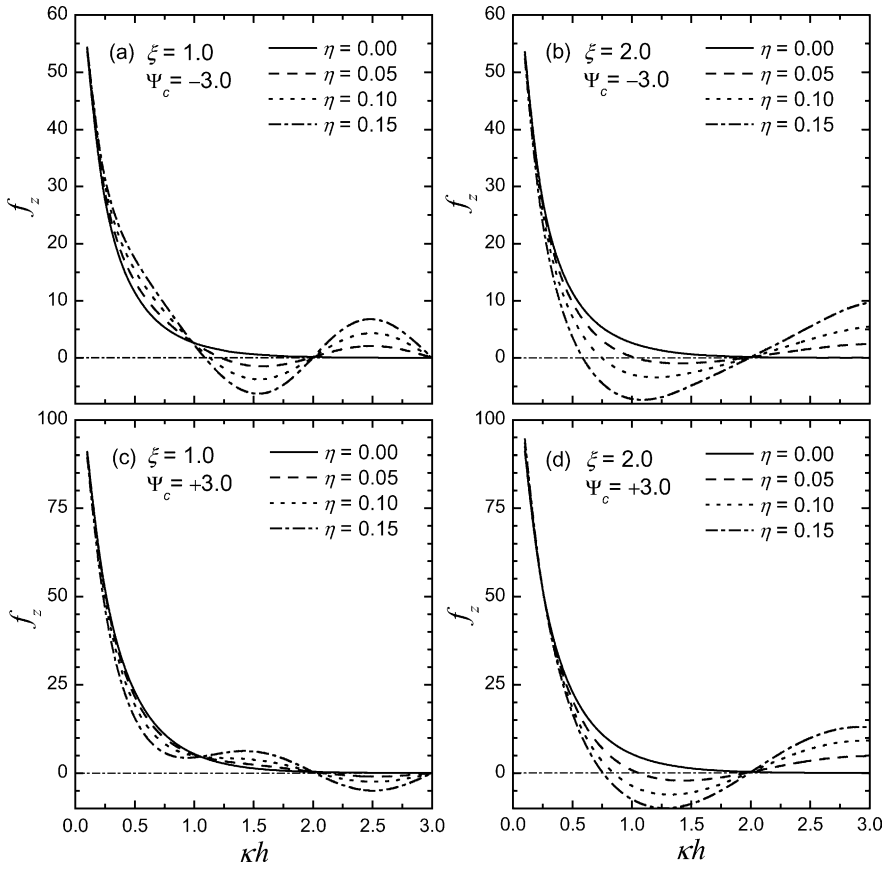

Fig. 3. Effect of the scaled amplitude of the roughness (η) on the particle–particle scaled electrostatic interaction force for two constant charge (CC) particles inside a constant potential (CP) rough capillary. The simulations were performed for four combinations of scaled wavelength (ξ) and scaled surface potential of the capillary wall (Ψ_c) as indicated in parts (a)–(d). The charge density on the particles was evaluated employing Eq. (6) assuming a surface potential $\Psi_{p,\infty} = -3.0$ on each particle at isolation. Different line types correspond to different values of scaled amplitude of the roughness as indicated in the legend.

at a point that coincides with the location of a crest of the capillary (point X in Fig. 1). All other finite separations were obtained by moving the particles away from point X symmetrically. This ensured that the effect of the capillary wall roughness is identical on the two particles.

In the subsequent sections, we provide the results obtained for different types of charging behavior on the particles, starting with the case of two CC particles inside a CP cylindrical capillary.

3. Constant charge particles inside a constant potential rough capillary

In this section, the electrostatic double layer forces between two constant charge (CC) particles inside a constant potential (CP) cylindrical capillary with embedded wall roughness are presented. Prior to presenting these results, however, the accuracy of the numerical solution is demonstrated by providing a comparison of the interaction force between two constant charge particles in an infinite medium (in absence of the capillary wall) obtained in this work with an independent numerical solution of the Poisson–Boltzmann equation.

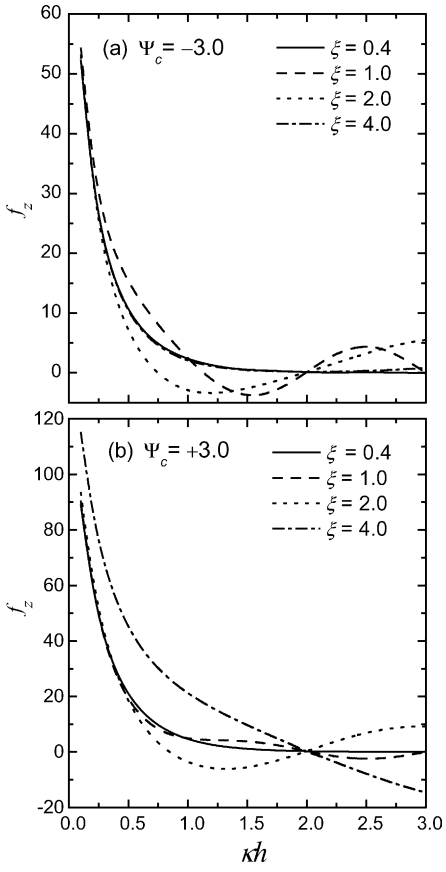

Fig. 4. Variations of the scaled electrostatic interaction force with scaled separation distance between the particles for different scaled wavelength (ξ) as indicated in the legend. Two parts of the figure represent two different surface potential of the capillary wall, namely, (a) $\Psi_c = -3.0$ and (b) $\Psi_c = +3.0$ for a fixed amplitude of the wall roughness ($\eta = 0.10$), while all other parameters are identical as Fig. 3.

3.1. Force between constant charge (CC) particles in an infinite medium

As mentioned earlier, the available studies in the literature mainly deal with the problem of particle–particle interaction in infinite media. To test the accuracy of the finite element results in the present work, we considered one of the limiting cases of the model, namely, interaction between two identical spherical particles in an infinite electrolyte medium. Here we assume that the capillary dimension is large enough compared to the particle dimensions so that the effect of the capillary is negligible on the net interaction between the particles. The interaction force is calculated without further modification of problem geometry or coordinate system. Furthermore, a Neumann boundary condition was applied on the cylinder wall (boundary IJ in Fig. 1):

$$\mathbf{n} \cdot \nabla \Psi = 0 \text{ on IJ} \tag{14}$$

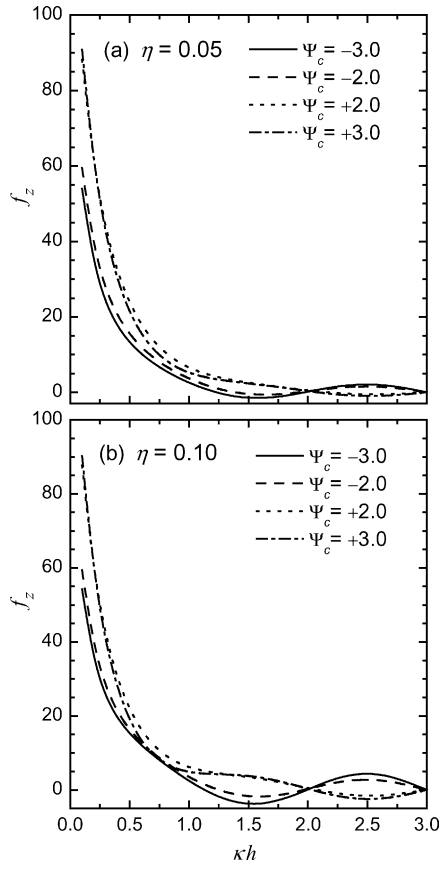

Fig. 5. Electrostatic interaction force between two CC particles corresponding to different surface potentials of the capillary for two values of scaled amplitude ($\eta = 0.05$ and 0.10). The variations of the scaled electrostatic force with scaled separation between the particles are depicted for a fixed value of scaled wavelength ($\xi = 1.0$) of the capillary, and a fixed value of scaled surface charge density (evaluated using $\Psi_{p,\infty} = -3.0$) for both particles. Different line types correspond to different values of scaled surface potential of the capillary wall as indicated in the legend.

A comparison of the interaction forces obtained from the finite element simulations with the corresponding numerical estimates obtained using a Hermite collocation technique for two constant charge particles interacting in an infinite electrolyte medium [16,20] is depicted in Fig. 2. The solid line represents the results from the Hermite collocation technique in a bi-spherical coordinate system while the symbols represent the results obtained from the finite element simulation in a cylindrical coordinate system. The interaction forces obtained from the finite element model are virtually identical to the collocation results over the entire range of scaled separation distances, $0 < \kappa h < 4$ (Fig. 2). Although the finite element results slightly deviate from the collocation results at larger separations, at small separations both results show a good agreement with each other. This implies that the numerical solution procedure employed in the present work provides reliable predictions of the EDL force.

It was also ensured that the results shown in this article are independent of the finite element mesh. The results obtained from different steps of the adaptive mesh refinement technique are given in Table 1 for the case of two constant charge spherical particles ($\Psi_{p,\infty} = -3$) inside a constant potential cylindrical capillary ($\Psi_c = -3$) at a fixed scaled separation distance, $\kappa h = 0.4$ between the particles. The results are shown for a smooth and a rough capillary. For the rough capillary simulations, the roughness is represented by the scaled wavelength and amplitude, defined as $\xi = \lambda/a$ and $\eta = \alpha/a$, respectively. From this table, it is clear that as we refine the mesh, the scaled EDL force (f_z) obtained from the numerical solution of the PB equation converge toward a fixed value. For $\eta = 0$ (smooth capillary), the results are within 0.02% of each other for the two highest number of elements. For a rough capillary ($\eta = 0.1$), convergence of the EDL forces is comparatively slower than the smooth capillary. This is mainly due to the fact that more elements are needed to accurately map the curved surfaces of the rough capillary wall. In case of rough capillaries, the forces tend to converge in an oscillatory manner, and results are within 0.1–0.2% for the two highest number of elements.

3.2. Force between constant charge (CC) particles inside constant potential (CP) rough capillary

The force acting in the axial direction on a spherical particle was determined for wide ranges of the surface roughness governed by the scaled amplitude of the roughness η (defined by amplitude/particle radius), and scaled pitch or wavelength ξ (the pitch of the undulations scaled with respect to particle

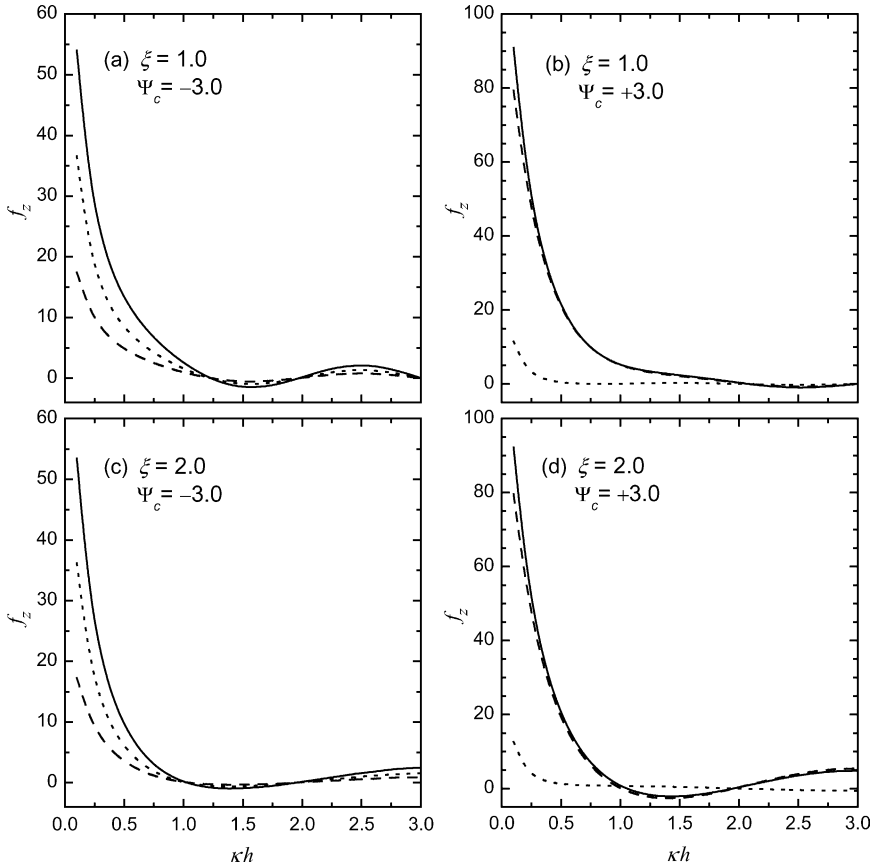

Fig. 6. Components of the scaled double layer interaction force as a function of scaled separation distance between the CC particles. The simulations were performed for a fixed value of scaled amplitude ($\eta = 0.05$), and a fixed value of scaled surface charge density (evaluated using $\Psi_{p,\infty} = -3.0$). All other conditions are shown in the figure legend. Three lines represent osmotic force (dotted lines), Maxwell force (dashed lines), and total EDL force (solid lines).

radius). Furthermore, a wide range of the scaled particle-particle separation distance κh, and various combinations of the surface potentials on the particle surface and capillary wall were explored, keeping the size ratio A (=b/a) constant. In the following, the influence of the surface roughness on the electrostatic interaction is discussed for different values of surface potentials on the cylindrical capillary.

Fig. 3 shows the variation of the interaction force between two constant charge (CC) spherical particles inside a rough cylindrical capillary with the scaled separation distance between the spherical particles (κh). In this figure, the forces are calculated for a fixed particle size ($\kappa a = 1$), a fixed value of the size ratio $A = b/a = 1.2$, and a fixed dimensionless surface potential on an isolated particle surface, $\Psi_{p,\infty} = -3$. The surface charge density on the particles was calculated using Eq. (6) based on the fixed surface potential of an isolated spherical particle. The results in Fig. 3a and b correspond to $\Psi_c = -3$ on the capillary wall, while the results in Fig. 3c and d correspond to $\Psi_c = +3$. In each part of Fig. 3, four curves are obtained corresponding to four values of the scaled amplitude, η, of the capillary wall roughness. Furthermore, the simulations were performed for two different values of the scaled wavelength, ξ, as indicated in each part of Fig. 3.

At small separations between the spherical particles, $\kappa h < 0.5$, the interaction forces between the particles remains relatively unaffected by the presence of the capillary wall. Neither the wall surface potential, nor the wall roughness influence the short range EDL interaction force between the particles. At larger separations, however, the effect of the capillary wall becomes more prominent on the EDL force. Strikingly, even similarly charged particles experience a periodically attractive and repulsive EDL force depending on the wavelength and amplitude of the wall roughness. At large separation between the particles, the oscillatory behavior of the interaction force is primarily an outcome of the interaction between the individual particles and the capillary wall. Overall, one observes a slight amplification in the magnitude of the interaction force when the cylinder wall potential has opposite sign to the particle surface potential. It is interesting to note from Fig. 3b and d, that altering the sign of the cylinder surface potential causes no qualitative changes in the oscillatory force profiles when the scaled wavelength of the wall roughness is 2. In other words, for roughness wavelengths greater than the particle size, the sign of the wall potential bears no consequence on the behavior of the EDL force between constant charge particles.

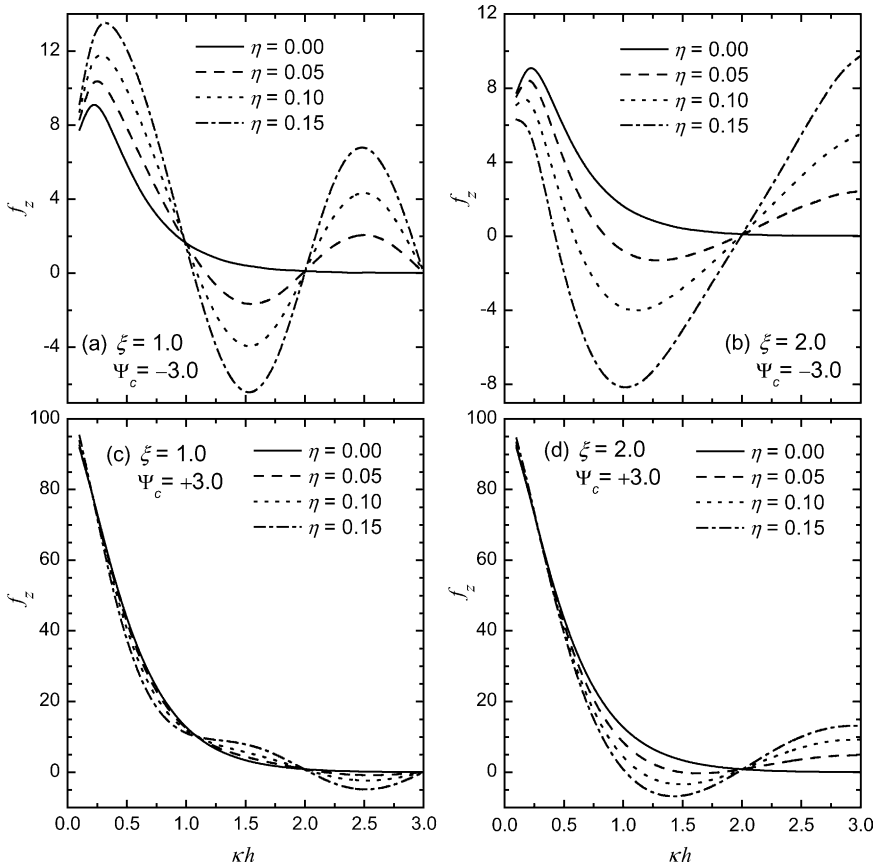

Fig. 7. Effect of the scaled amplitude of the roughness (η) on the scaled electrostatic interaction force experienced by a constant charge (CC) particle while interacting with a constant potential (CP) particle inside a constant potential (CP) rough capillary. The scaled electrostatic force is calculated for two scaled wavelengths (ξ) and two scaled surface potentials of the CP capillary (Ψ_c). The charge density of the CC particle is obtained using an isolated particle potential of −3 in Eq. (6) while the surface potential of the CP particle is set to −3. Other simulation parameters are identical as Fig. 3.

This happens for constant potential conditions on the cylinder wall.

The influence of varying the wavelength of the capillary wall roughness on the interaction force is depicted in Fig. 4. In these simulations, the amplitude of the wall roughness was fixed at 0.1. The forces corresponding two four values of the wavelength are depicted in Fig. 4a and b. In all the simulations, the particle surface potential was set at −3. Fig. 4a shows the scaled forces when the capillary wall surface potential is −3. In this case, the interaction force is not influenced by the roughness when the wavelength is smaller ($\xi = 0.4$) than the particle radius. For intermediate wavelengths, the interaction force becomes oscillatory reflecting the periodicity of the capillary wall roughness. When the cylinder wall surface potential is +3 (Fig. 4b), the interaction force magnitudes increase substantially, and we observe a considerable influence of the wall geometry on the EDL forces. Notably, for $\xi = 4$, the decay behavior of the interaction force becomes considerably different from the remaining force profiles.

The effect of different capillary wall surface potentials on the EDL interaction between two CC particles is depicted in Fig. 5. All simulation conditions are shown in the figure legend and caption. These figures indicate that changing the sign of the dimensionless surface potential of the capillary wall (Ψ_c) induces a significant change of repulsive force between the particles at small separations. For $\eta = 0.1$, effect of the surface potential is more prominent at large separation distances than $\eta = 0.05$. However, changing the magnitude of the potential keeping the sign unchanged did not show any significant change on the interaction force.

In summary, the interaction force profiles show remarkably varied trends depending on the roughness and surface potential of the confining geometry. For constant charge particles, one might find such variations of the force, particularly, the presence of attractive interactions between two identically charged particles, quite counterintuitive. However, closer inspection of the components of the total force, namely, the osmotic stress and the Maxwell stresses, reveals that such oscillations are entirely feasible in such confined geometries. This is at least mathematically consistent in the framework of the Poisson–Boltzmann model and its assumptions. Fig. 6 depicts a few representative cases, where the total force on a particle and its two components (osmotic and Maxwell forces) are shown for different combinations of wall roughness and wall surface potentials. In these simulations, the isolated particle surface potential is set to −3. Fig. 6a and b show the results for a roughness wavelength (ξ) of 1 while Fig. 6c and d depict the forces for $\xi = 2$. Comparing Fig. 6a with b, as well as 6c with 6d, we note that changing the sign of the cylinder surface potential alters the dominating influence of osmotic and Maxwell stresses on the total EDL force. When the particle and cylinder surface potentials are of the same sign, the osmotic stress contribution dominates, while for opposite signs of these surface potentials, the Maxwell stress becomes the dominant contributor to the total interaction force. It is thus evident that for constant charge particles, the EDL forces are susceptible to tremendous influence of the confining domain as the separation between the particles increases. It was noted in our earlier work [24] that for constant potential particles, the entire contribution to the EDL force comes from Maxwell stresses, since the osmotic stress on the constant potential particle surface vanishes upon integration. In the present simulations, we note that the osmotic stresses become negligible only when the confining walls of the capillary have a surface potential of opposite sign to the particles.

4. Interaction between constant charge and constant potential particles

In this section, we focus on the case when the two confined particles have different types charging properties, namely, constant potential and constant surface charge density. Here, the surface of one particle (sphere BCD) is assigned a constant surface charge density as Eq. (4) while the other particle (sphere EFG) is assigned a constant potential of Ψ_p, (Eq. (9)). The capillary wall is subjected to a constant potential of Ψ_c.

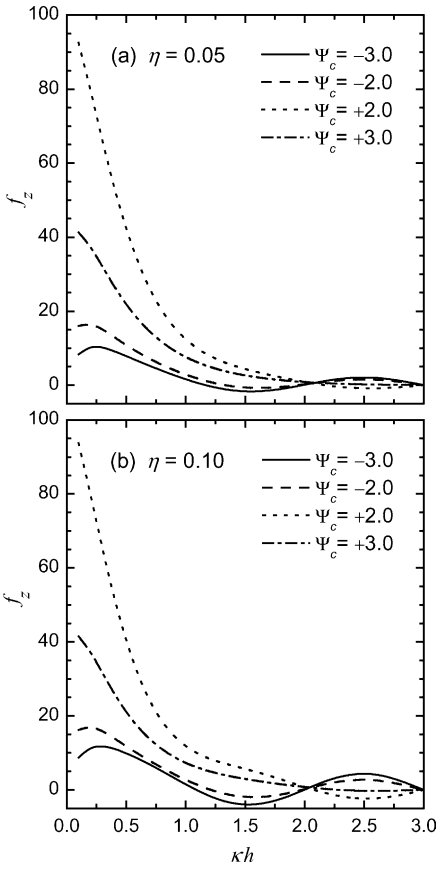

Fig. 8. Variations of the scaled interaction force experienced by a CC particle interacting with a CP particle in a constant potential rough capillary. Two parts represent the results for two values of scaled amplitude ($\eta = 0.05$ and 0.10) and a fixed dimensionless wavelength ($\xi = 1.0$). The scaled surface potential of the CP particle and the scaled surface charge density of the CC particle are identical to those used in Fig. 7.

The potential on the isolated CC particle as well as the CP particle were set to −3 in these simulations. Other simulation parameters are identical to those used in Fig. 3.

4.1. Force experienced by constant charge (CC) particle

We first focus on the net force experienced by a CC particle in presence of the CP capillary wall and a CP particle. Fig. 7 depicts the variation of the interaction force experienced by the constant charge spherical particle for this case with the scaled separation distance between the particles (κh). The results were obtained for four values of scaled amplitude, namely, $\eta = 0, 0.05, 0.1$, and 0.15 of the roughness. Fig. 7a and b show the scaled electrostatic forces for scaled wavelengths of $\xi = 1$ and 2, respectively, while keeping the capillary surface potential −3 (same sign and magnitude as the surface potential on the isolated particles). Fig. 7c and d show the corresponding forces when the scaled capillary potential is +3 (opposite in sign compared to the potential on an isolated spherical particle).

The force experienced by the CC particle in Fig. 7a and b are significantly lower than the corresponding forces in Fig. 7c and d. This implies that the potential of the capillary wall, coupled with the presence of a CP particle in the vicinity will drastically alter the force experienced by the CC particle. Notably, for the case of two interacting CC particles in a capillary, the short-range force was generally unaffected by the capillary wall potential (Fig. 3). When the surface potential of the capillary wall is switched to +3 (Fig. 7c and d), the interaction force on the CC particle becomes largely repulsive for small values of κh. In fact the results in Fig. 7c and d are almost identical to those observed for the interaction between two CC particles in Fig. 3c and d. Thus, the force experienced by the CC particle is strongly influenced by the magnitude and sign of the surface potential of the capillary wall.

This dependence of the force experienced by the CC particle on the capillary wall surface potential is depicted more clearly in Fig. 8. Here, we observe that the interaction force for small values of κh dramatically increases (becomes more repulsive) as the capillary wall potential is varied from −3 to +3. Notably, the forces do not seem to depend strongly on the amplitude of the capillary wall roughness as observed by comparing the forces from Fig. 8a and b. Only at larger separations do we see some influence of the roughness amplitude on the interaction force.

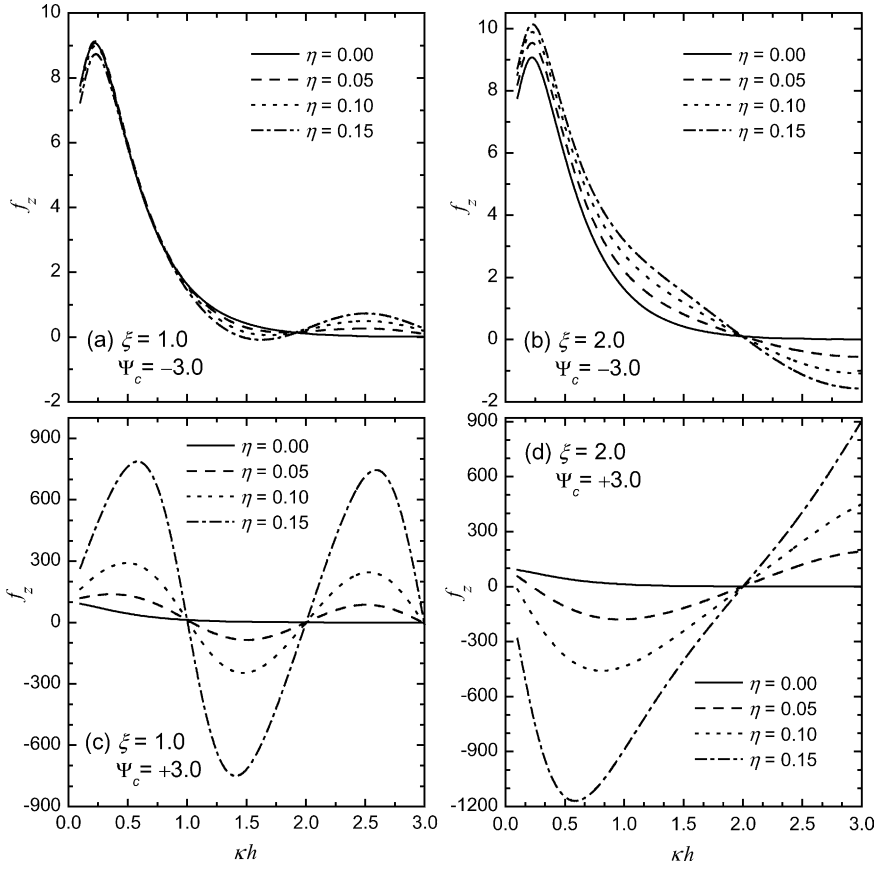

Fig. 9. Effect of the scaled amplitude of the roughness (η) on the scaled electrostatic interaction force experienced by a constant potential (CP) particle while interacting with a constant charge (CC) particle inside a constant potential (CP) rough capillary. All other conditions are identical as Fig. 7, except that the integration of the total stress tensor is performed over the CP particle (surface EFG in Fig. 1).

4.2. Force experienced by constant potential (CP) particle

We now turn our attention to the forces experienced by the CP particle in the same system. The interaction forces experienced by the CP particle are shown in Fig. 9. All conditions and parameters in Fig. 9 are identical to those in Fig. 7, excepting the calculation of the forces, which are now performed by integrating the stress tensor over the surface of the CP particle (sphere EFG).

For identical sets of parameters, the force experienced by the CP particle is significantly lower when the surface potential of the capillary wall is −3 (Fig. 9a and b) as opposed to when the capillary wall surface potential is +3 (Fig. 9c and d). The forces are dramatically enhanced when the capillary wall potential is opposite in sign to the particle surface potential. Considering the fact that for a CP particle, the isotropic osmotic stress, integrated over the particle surface vanishes, this enormous fluctuation of the net force is solely the outcome of the largely unbalanced Maxwell stresses acting on the particle. We note that the force indeed passes through zero when the particle is symmetrically located at the crest or trough of an undulation in the capillary wall.

One should note that in these simulations, the distance between the particles is varied by symmetrically moving the particles away from the center of the capillary (point X in Fig. 1), such that both particles are equidistant from the starting point at any given separation. This implies that the forces experienced by each particle should be identical. This was observed in the simulations for two CC particles, where integration of the stress tensor over both particles provided the same force. Comparing Figs. 7 and 9, however we observe a vastly different interaction force on the CC and CP particles in rough capillaries. A closer inspection of the solid lines in Figs. 7 and 9 reveal that when the capillary wall has no roughness, the force experienced by the CC and the CP particles are identical. Therefore, the large difference between the forces seen on the CC and CP particles inside rough capillaries solely arises due to the roughness and the surface potential of the capillary wall. The capillary wall affects the stress tensor differently on the CC and CP particles, yielding different magnitudes of the force on them.

Fig. 10 depicts the variation of the interaction force on the CP particle with different surface potentials on the capillary wall. When both the capillary and particle surface potentials bear similar signs, the force on the CP particle is marginally affected. However, if the capillary wall surface potential is opposite in sign to the particle potential, we observe large oscillations in the interaction force. In summary, presence of roughness appears to induce a significant oscillation in the forces experienced by a CP particle, which alternately become attractive and repulsive, emulating the periodic nature of the roughness. This effect is particularly pronounced when the surface potentials on the particle and the capillary wall have opposite signs.

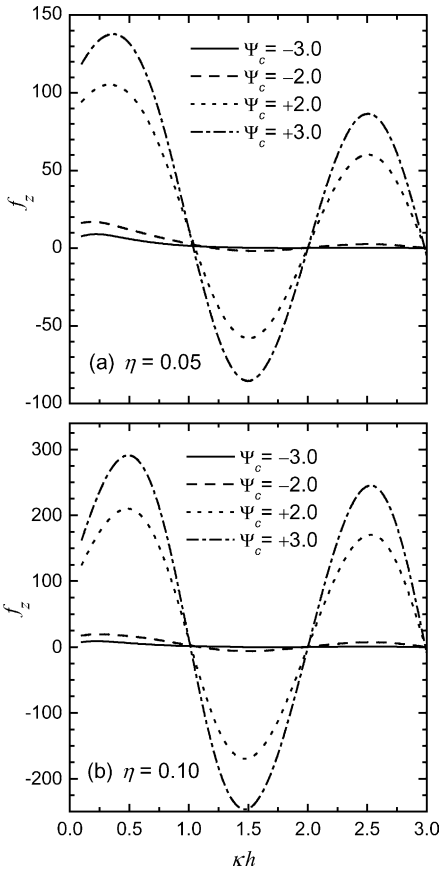

Fig. 10. Variations of the scaled interaction force experienced by a CP particle interacting with a CC particle in a CP capillary for different surface potentials of the capillary. The two parts of the figure represent the results for two values of scaled amplitude (η = 0.05 and 0.10) and a fixed dimensionless wavelength (ξ = 1.0). The scaled surface potential of the CP particle and the scaled surface charge density of the CC particle are identical to those used in Fig. 7.

5. Constant charge particles inside constant charge rough capillary

The interaction forces were presented so far for the situations where the capillary wall had a constant surface potential. Results for constant charge density on the capillary wall are presented in this section. Here, both particles as well as the capillary wall are assigned a constant surface charge density. While the particle charge densities are assigned using Eq. (6) and a given surface potential at isolation, the capillary wall charge density is assigned different values arbitrarily.

The effect of the constant charge rough capillary on the interaction forces between two CC particles is shown in Fig. 11. The simulations were performed under identical conditions as in Fig. 3, except for constant surface charge density conditions on the capillary wall. The results in Fig. 11a and b correspond to the case when the scaled surface charge density on the capillary wall is $\sigma_c = -6.8$ (equal to the particles surface charge density, σ_p), while the results in Fig. 11c and d correspond to $\sigma_c = +6.8$. Typically, for 0.001 M symmetric (1:1) electrolyte solution, $\sigma_c = 6.8$ corresponds to

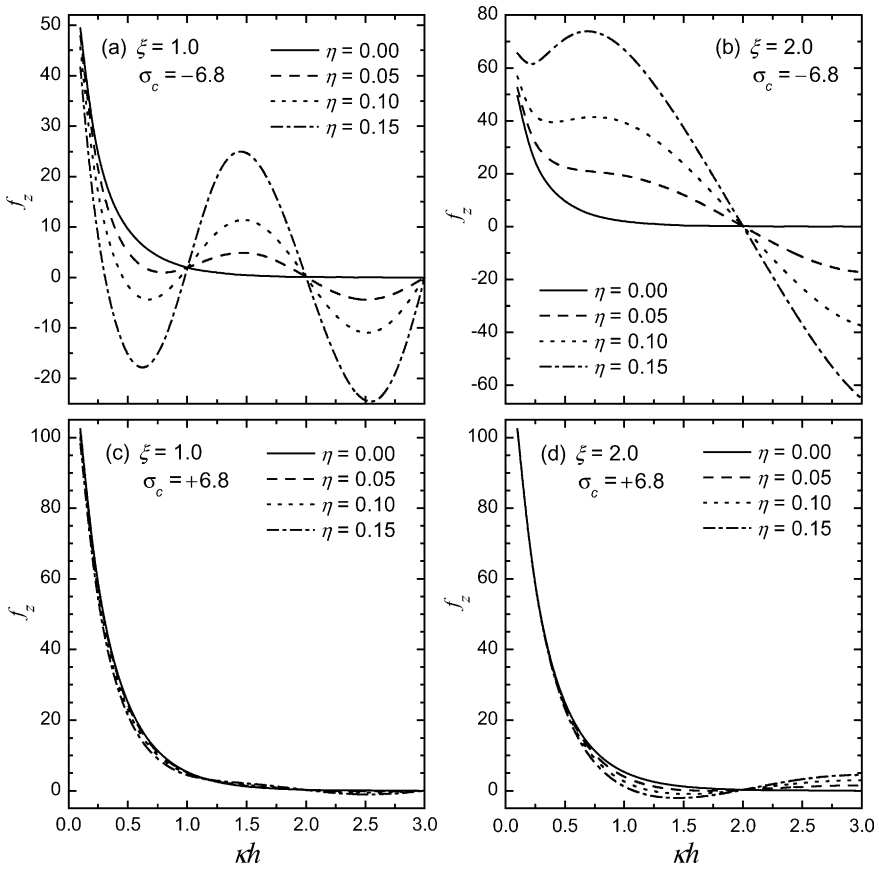

Fig. 11. Effect of the scaled amplitude of the roughness (η) on the particle–particle scaled electrostatic interaction force for two constant charge (CC) particles inside a constant charge (CC) rough capillary. The simulations were performed for combinations of two scaled wavelengths (ξ) and two scaled surface charge densities of the capillary wall (σ_c). The scaled surface charge density of the CC particles is same as in Fig. 3. Different line types correspond to different values of scaled amplitude of the roughness as indicated in the legend.

1.26×10^{-2} C m^{-2}. When the scaled capillary wall charge density is −6.8, the interaction force on the CC particles oscillates considerably between positive and negative values, emulating the periodic nature of the roughness of the capillary. However, when the capillary wall charge density is +6.8, the influence of surface roughness on the force becomes almost negligible at small separation distances between the particles. In particular, when the wavelength of the wall roughness is comparable to the particle radius, the interaction force does not depict any perceptible oscillatory nature even at large separations.

The results of Fig. 11 depict that even when all the surfaces are similarly charged, and exhibit constant charge properties, the confined particles can experience localized oscillations in the interaction force owing to the presence of the rough wall. The interaction force can attain fairly large negative values (attraction) as shown in Fig. 11b. It is therefore discernable that the EDL interaction between similarly charged particles in narrow rough capillaries can become attractive under a variety of conditions even within the framework of the classical Poisson–Boltzmann equation. This behavior is of course never observed in absence of capillary wall roughness.

6. Summary and conclusions

The interaction force experienced by particles with different charging behaviors in a rough capillary exhibit a remarkably diverse nature. The roughness of the capillary wall, manifested by two parameters (amplitude and wavelength), coupled with the surface charging behavior can render the forces on the particles attractive or repulsive. The three scenarios explored in this study, namely, two CC particles in a CP capillary, a CC and a CP particle in a CP capillary, and two CC particles in a CC capillary, provide the following key observations. First, the enormous variability of the forces is a consequence of variation of both Maxwell and osmotic stresses on the CC particles. In case of CP particles, this is solely due to the variation of the Maxwell stresses. Secondly, the force experienced by the CC and CP particles are quite different when they are trapped together in a rough cylindrical capillary. Thirdly, the effect of roughness is pronounced only when the roughness wavelength is comparable to or larger than the particle size. Finally, the capillary wall surface potential and its charging behavior (constant potential or constant surface charge density) have tremendous influence on the force experienced by the particles.

The huge fluctuations in the forces, and the ability to affect significant variations in these forces by altering the capillary wall geometry and its surface potential (or surface charge density), seem to be an attractive means for development of actuation mechanisms in micro- or nano-fluidic devices. While certainly these effects will not be perceptible in case of large particles (large κa) or very small roughness amplitudes compared to the particles, it is entirely possible to obtain systems with κa values close to 1. For most non-aqueous systems, the dielectric constant of the solvent can be significantly smaller than that of water, and consequently, smaller values of κa can be achieved with fairly large particles in such solvents. Furthermore, solubility of ions is significantly smaller in many such solvents, resulting in extremely long-range EDL interactions. Thus, manipulating EDL forces on colloidal particles in narrow cylindrical channels can be of immense significance in a variety of applications related to micro-scale separations, flow control devices, porous media transport, and analytical systems.

The periodic nature of the oscillations in capillary wall geometry modeled in this study can emulate a peristaltic motion of a "soft" capillary wall. It is apparent from our calculations that such peristaltic motion coupled with an appropriate charging behavior can be effectively used to impart an axial motion of the particles trapped inside the capillary in a controlled manner. The implications of such induced movement of the particles is far reaching. On one hand, this mechanism can be used to induce coagulation of two particles, while on the other hand the mechanism can be exploited to transport particles through the capillary in a controlled manner.

Acknowledgements

The authors wish to acknowledge the Alberta Ingenuity Fund and the Canada Research Chairs (CRC) program for financial support. P.K.D. also acknowledges financial support from Alberta Ingenuity Fund Studentship Award and Izaak Walton Killam Memorial Scholarship.

References

[1] B.V. Derjaguin, L. Landau, Acta Physicochim. (USSR) 14 (1941) 633.
[2] E.J. Verwey, J.T.G. Overbeek, Theory of Stability of Lyophobic Colloids, Elsevier, Amsterdam, 1948.
[3] J.H. Masliyah, Electrokinetic Transport Phenomena, AOSTRA, Edmonton, 1994.
[4] M. Elimelech, J. Gregory, X. Jia, R. Williams, Particle Deposition and Aggregation: Measurement, Modelling and Simulation, Butterworth–Heinemann, Oxford, 1995.
[5] H. Tamai, Y. Nagai, T. Suzawa, J. Colloid Interf. Sci. 91 (1983) 464.
[6] J. Czarnecki, Adv. Colloid Interf. Sci. 24 (1986) 283.
[7] J. Czarnecki, P. Warszynski, Colloids Surf. 22 (1987) 207.
[8] J.E. Tobiason, Colloids Surf. 39 (1989) 53.
[9] M. Elimelech, C.R. Omelia, Langmuir 6 (1990) 1153.
[10] S.Y. Shulepov, G. Frens, J. Colloid Interf. Sci. 170 (1995) 44.
[11] S.Y. Shulepov, G. Frens, J. Colloid Interf. Sci. 182 (1996) 388.
[12] J.Y. Walz, Adv. Colloid Interf. Sci. 74 (1998) 119.
[13] S.L. Carnie, D.Y.C. Chan, J. Colloid Interf. Sci. 155 (1993) 297.
[14] S.L. Carnie, D.Y.C. Chan, J. Colloid Interf. Sci. 161 (1993) 260.
[15] S.L. Carnie, D.Y.C. Chan, J.S. Gunning, Langmuir 10 (1994) 2993.
[16] S.L. Carnie, D.Y.C. Chan, J. Stankovich, J. Colloid Interf. Sci. 165 (1994) 116.
[17] H. Ohshima, J. Colloid Interf. Sci. 168 (1994) 255.
[18] H. Ohshima, Adv. Colloid Interf. Sci. 53 (1994) 77.
[19] D. Mccormack, S.L. Carnie, D.Y.C. Chan, J. Colloid Interf. Sci. 169 (1995) 177.
[20] J. Stankovich, S.L. Carnie, Langmuir 12 (1996) 1453.
[21] P. Warszynski, Z. Adamczyk, J. Colloid Interf. Sci. 187 (1997) 283.
[22] H. Ohshima, Colloid. Polym. Sci. 277 (1999) 563.
[23] P.K. Das, S. Bhattacharjee, W. Moussa, Langmuir 19 (2003) 4162.
[24] P.K. Das, S. Bhattacharjee, J. Colloid Interf. Sci. 273 (2004) 278.
[25] J.L.M. Vanbree, J.A. Poulis, B.J. Verhaar, K. Schram, Physica 78 (1974) 187.
[26] J. Czarnecki, T. Dabros, J. Colloid Interf. Sci. 78 (1980) 25.
[27] J. Czarnecki, V. Itschenskij, J. Colloid Interf. Sci. 98 (1984) 590.
[28] M.C. Herman, K.D. Papadopoulos, J. Colloid Interf. Sci. 136 (1990) 385.
[29] M.C. Herman, K.D. Papadopoulos, J. Colloid Interf. Sci. 142 (1991) 331.
[30] R.F. Probstein, Physicochemical Hydrodynamics: An Introduction, Wiley, New Jersey, 2003.
[31] J.E. Sader, D.Y.C. Chan, Langmuir 16 (2000) 324.
[32] W.B. Russel, D.A. Saville, W.R. Schowalter, Colloidal Dispersions, Cambridge University Press, New York, 1989.